Volume 12, Issue 3, Page 128-133, 2023 https://doi.org/10.46810/tdfd.132635 Research Article

BİNGÖL ÜNİVERSİTESİ

Türk Doğa ve Fen Dergisi
Turkish Journal of Nature and Science

www.dergipark.gov.tr/tdfd

Synthesis of $Li_7P_3S_{11}$ Solid Electrolyte for All-Solid-State Lithium-Sulfur Batteries

Çağrı Gökhan TÜRK[1,2], Mahmud TOKUR[2,3,4*]

[1]Sakarya University, Institute of Natural Sciences, Sakarya, Türkiye
[2]Sakarya University, Research, Development and Application Center, Sakarya, Türkiye
[3]Sakarya University, Department of Metallurgical & Materials Engineering, Sakarya, Türkiye
[4]NESSTEC Energy & Surface Technologies A.S., Technology Development Zones, Sakarya, Türkiye
Çağrı Gökhan TÜRK ORCID No: 0000-0001-9940-6948
Mahmud TOKUR ORCID No: 0000-0003-3612-5350

**Corresponding author: mtokur@sakarya.edu.tr*

(Received: 12.07.2023, Accepted: 13.09.2023, Online Publication: 27.09.2023)

Keywords
Energy storage, Lithium-Sulfur battery, $Li_7P_3S_{11}$ solid electrolyte

Abstract: Solid electrolytes containing sulfur are gaining increasing traction among researchers and are growing in popularity with each passing day. Recently, $Li_7P_3S_{11}$, $Li_{10}GeP_2S_{12}$, and $Li_{11}Si_2PS_{12}$ solid electrolytes have been of great interest in literature. The ionic conductivity of these electrolytes can attain a value as high as 10^{-2} S/cm. For this purpose, this study employed the mechanical alloying method to synthesize the $Li_7P_3S_{11}$ solid electrolyte for use in all-solid-state lithium-sulfur batteries. To accomplish this, Li_2S and P_2S_5 ingredients were mixed in a ball mill at certain stoichiometric ratios. The crystallization temperatures of the obtained powders were determined by the DSC thermal analysis method, and they were crystallized under a protective atmosphere at the appropriate crystallization temperature. Subsequently, the acquired powders, known for their high sensitivity to ambient conditions, underwent XRD and Raman analysis within a specially designed enclosure to prevent exposure to open atmosphere. Powders that underwent structural characterization were subjected to electrochemical testing through electrochemical impedance spectroscopy and cyclic voltammetry analyses in a special solid-state cell. Notably, the cyclic voltammetry analysis unveiled an impressive electrochemical window extending to a minimum of 5 V. Additionally, the total conductivity of the $Li_7P_3S_{11}$ pellet was quantified at 1.1 mS cm^{-1} at room temperature, further emphasizing its favorable electrochemical properties. The results exhibited compatibility with existing literature, confirming the synthesized electrolyte's viability as a fitting candidate for lithium-sulfur batteries.

Tam Katı Hal Lityum-Sülfür Piller için $Li_7P_3S_{11}$ Katı Elektrolit Sentezi

Anahtar Kelimeler
Enerji depolama, Lityum-Sülfür pil, $Li_7P_3S_{11}$ Katı elektrolit

Öz: Sülfür içeren katı elektrolitler, bilim insanları için oldukça caziptir ve her geçen gün cazibesi artmaktadır. Son zamanlarda $Li_7P_3S_{11}$, $Li_{10}GeP_2S_{12}$ ve $Li_{11}Si_2PS_{12}$ katı elektrolitleri literatürde büyük ilgi görmektedir. Bu elektrolitlerin iyonik iletkenliği 10^{-2} S/cm seviyelerine bile ulaşabilmektedir. Bu amaçla, bu çalışmada tamamen katı hal Lityum Sülfür piller için mekanik alaşımlama yöntemi ile $Li_7P_3S_{11}$ katı elektroliti sentezlenmiştir. Bunun için Li_2S ve P_2S_5 bileşenleri bir bilyalı değirmende belirli stokiyometrik oranlarda karıştırılmıştır. Elde edilen tozların kristalleşme sıcaklıkları DSC termal analiz yöntemi ile belirlenmiş ve uygun kristalleşme sıcaklığında koruyucu atmosfer altında kristallendirilmiştir. Daha sonra elde edilen ve açık atmosfere karşı oldukça hassas olan tozlar özel yapım bir tutucu ile XRD ve Raman analizine tabi tutulmuştur. Yapısal olarak karakterize edilen tozlar, özel bir katı hal hücresinde elektrokimyasal empedans spektroskopisi ve çevrimsel voltammetri analizleri ile elektrokimyasal olarak test edilmiştir. Sonuçların literatürle uyumlu olduğu görülmüş ve sentezlenen elektrolitin lityum sülfür piller için uygun bir aday olarak kullanılabileceği belirlenmiştir.

1. INTRODUCTION

Elemental sulfur (S) is emerging as a captivating contender for the cathode component of batteries, exhibiting promising outcomes in the realm of next-generation battery technologies. The non-toxic and environmentally benign nature of sulfur, coupled with its abundant presence in nature and cost-effectiveness, amplifies its allure for next-generation technologies and further clears the path ahead. With a theoretical capacity of 1675 mAh g^{-1} and an impressive energy density of 2567 Wh kg^{-1}, lithium-sulfur batteries outshine today's established commercial Li-ion batteries by a factor of five in terms of specific energy density [1]. Hence, lithium-sulfur batteries stand as a remarkable substitute for lithium-ion batteries in the future, with their operational mechanisms closely resembling those of conventional battery technologies [2].

Nevertheless, the commercial implementation of lithium-sulfur continues to face challenges when incorporating their active materials within liquid electrolyte environments. Primarily, the shuttle effect which stems from the dissolution of undesired lithium polysulfide intermediates into the lithium anode through the electrolyte and separator. This occurrence leads to diminished capacity and swift capacity deterioration [3-5].

In recent years, solid-state batteries (SSBs) have emerged as a compelling solution to address the enduring challenges in energy storage [6]. What sets solid-state lithium-sulfur batteries apart from their traditional counterparts is their reliance on a singular, robust sulfide electrolyte characterized by an exceptionally high ionic conductivity, effectively supplanting the conventional combination of liquid electrolytes and separators.

Among these sulfide electrolytes, the "simple" $Li_2S - P_2S$ binary system, collectively known as the $Li_7P_3S_{11}$ family, has garnered significant attention due to its remarkable properties [6]. These $Li_7P_3S_{11}$ materials exhibit extraordinary conductivity levels (> 10^{-4} Scm^{-1}) without the need for additional elements like Si, Ge, or Al [7]. Various crystalline and amorphous materials within the $Li_7P_3S_{11}$ family have been synthesized using diverse techniques, including the ball milling method, heat treatment, hot pressing, wet chemical treatment [8, 9], and more [10-12]. The key advantages of solid electrolytes lie in their capacity to dramatically enhance the power density of electrochemical cells, primarily due to their exceptional ionic conductivity. Additionally, they offer a heightened level of safety. Moreover, solid electrolytes present a promising solution to mitigate the shuttle effect, a persistent issue in lithium-sulfur batteries [6, 13].

Nevertheless, certain challenges persist, particularly related to lithium-ion diffusion kinetics, the electrode-electrolyte interface, and overall electrochemical performance. The adoption of solid electrolytes may introduce interface challenges between the electrolyte and electrodes, potentially impacting both ionic and electrical conductivity, and thereby potentially affecting the cell's capacity and stability [14].

In the context of this study, we synthesized a high-ionic-conductivity solid electrolyte, $Li_7P_3S_{11}$, using the meticulous blending of specific quantities of Li_2S and P_2S_5 constituents through the ball milling method. Subsequent comprehensive structural and electrochemical assessments revealed highly promising results. These findings make a substantial and meaningful contribution to the scientific literature, underscoring the significant potential of $Li_7P_3S_{11}$ for applications in all-solid-state lithium-sulfur batteries.

2. EXPERIMENTAL STUDIES

The production of triclinic sulfur-based solid electrolyte $Li_7P_3S_{11}$ was carried out in two stages. Li_2S and P_2S_5 powders were mixed into the ball mill at specific ratios (3:7 according to their atomic weights) in a special atmosphere-controlled mortar (in the glovebox) without exposure to air. The synthesis of the triclinic sulfur-based solid electrolyte $Li_7P_3S_{11}$ was carried out in a dual-stage process. Li_2S and P_2S_5 powders were meticulously combined in a ball mill, following specific ratios (3:7 based on their atomic weights), within a controlled atmosphere (inside a glovebox) to prevent air exposure. Subsequently, the mechanical activation process was conducted at 600 rpm for a duration of 15 hours. This procedure resulted in the formation of amorphous $Li_7P_3S_{11}$. The ball-milled glassy powders were then placed within a sealed quartz tube and subjected to sintering at 265°C for a span of 2 hours. Finally, the result was the successful production of a crystalline solid electrolyte, $Li_7P_3S_{11}$. Structural analysis of the synthesized glass-ceramic powders was carried out by X-ray diffraction (RigakuD/MAX2000) and Raman with custom-made kapton band-sealed apparatus. DSC analysis was conducted before crystallization heat treatment to characterize the possible exo (endo) thermic reactions during synthesis. Electrochemical tests were conducted at the GAMRY workstation. 100 mg of optimized solid electrolyte powders were put into a PEEK-insulated die with a 10 mm diameter and pressed under 400 Mpa. Solid state cell was then assembled by loading indium on both sides of the $Li_7P_3S_{11}$ pellet and pressing again for the electrochemical impedance test (symmetrical In/$Li_7P_3S_{11}$/In) at a frequency between 1 MHz - 1 Hz with 10 mV amplitude. Cyclic Voltammetry (CV) tests were conducted by asymmetrical Li/ $Li_7P_3S_{11}$/Stainless Steel cell between -0.01 V and 4.5 V (vs. Li/Li^+) with 1 mV/s step size to evaluate the electrochemical window of the synthesized solid electrolyte.

3. RESULTS AND DISCUSSIONS

To investigate the crystallographic properties of the obtained powders, XRD analysis was conducted, shown in Figure 1. Scanning was carried out between 10° and 40° with a scan rate of 1°/min. Compared to the other $Li_7P_3S_{11}$ structures from the reported studies, narrower

peaks were observed in the XRD analyses in this study instead of the wide peaks. The main peak for $Li_7P_3S_{11}$ at 30° after the sintering process, also in agreement with the literature [9, 15]. The phase formation of obtained powder shows crystalline character due to the milling energy of the phase in the (211) plane [16].

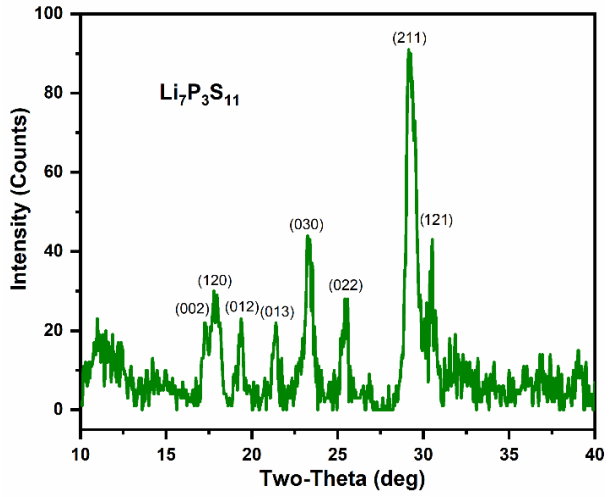

Figure 1. XRD analysis of $Li_7P_3S_{11}$ glass ceramic.

To characterize particle morphology and size, SEM analysis was employed, as depicted in Figure 2, providing SEM image of the $Li_7P_3S_{11}$ solid electrolyte. The particle size of $Li_7P_3S_{11}$ was found to exceed 700 nm, indicating that small particles of Li_2S and P_2S_5 are incorporated into the larger $Li_7P_3S_{11}$ structure and undergo crystalline transformation, consistent with the XRD results. This observation also suggests a homogeneous mixing of solid electrolyte composites. Thus, the results confirm the uniformity in the blending of Li_2S and P_2S_5 materials.

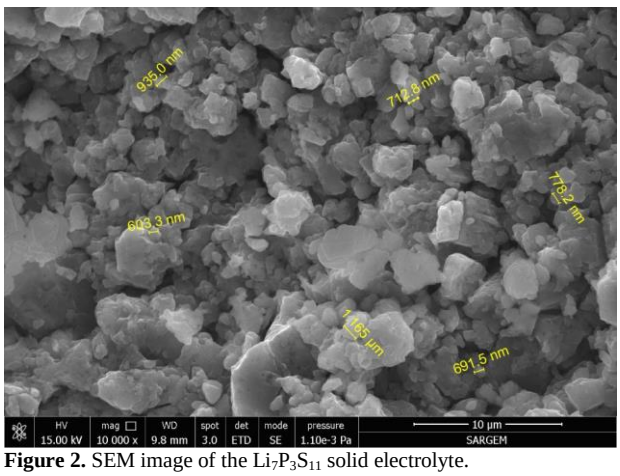

Figure 2. SEM image of the $Li_7P_3S_{11}$ solid electrolyte.

DSC analysis was carried out in order to determine the crystallization temperature of amorphous $Li_7P_3S_{11}$ powders, as shown in Figure 3. DSC can measure the amount of absorbed or released energy while the sample is heated, cooled, or kept at a constant temperature [17, 18]. In this technique, the temperature difference between the reference and the sample is shown depending on temperature or time [18]. Amorphous or irregular undesirable structures may occur below or above the crystallization temperature. Therefore, it is an important step to determine the transition temperature from amorphous to crystalline structure [19, 20]. As a result of the DSC analysis, two peaks are raised between 250 °C and 350 °C, which indicates the existence of two exothermic reactions that characterize the crystallization of the $Li_7P_3S_{11}$ and $Li_4P_2S_6$ phases [21]. It is extremely important to define these peaks in order to know what kind of compounds can be obtained at certain temperatures. The peak of the targeted appropriate structure of $Li_7P_3S_{11}$ formed at about 260 °C.

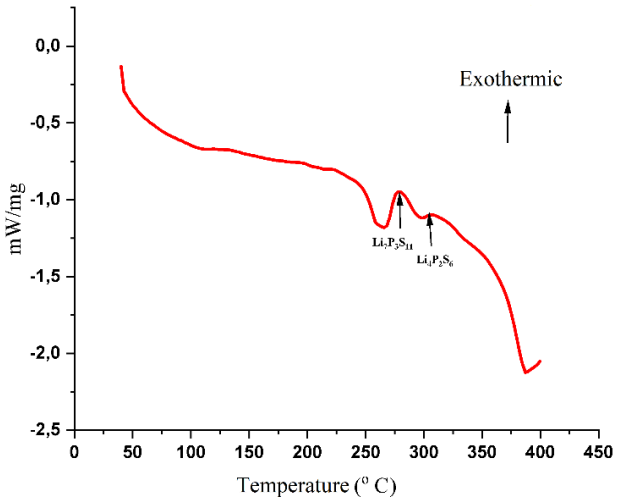

Figure 3. DSC analysis of amorphous $Li_7P_3S_{11}$ powders.

Differences in the wavelength of the light interacting with the molecule create Raman shifts [22]. These differences give information about the chemical properties of the molecules. Raman analyses of $Li_7P_3S_{11}$ powders are given in Figure 4. The atomic local environment in the $Li_7P_3S_{11}$ structure consists of PS_4^{-3} tetrahedra and $P_2S_7^{-4}$ ditetrahedra. As is known, $P_2S_7^{-4}$ is a metastable phase and tends to transform into $P_2S_6^{-4}$ [23].

$$P_2S_7^{-4} = P_2S_6^{-4} + 1/8\ S_8 \quad (1)$$

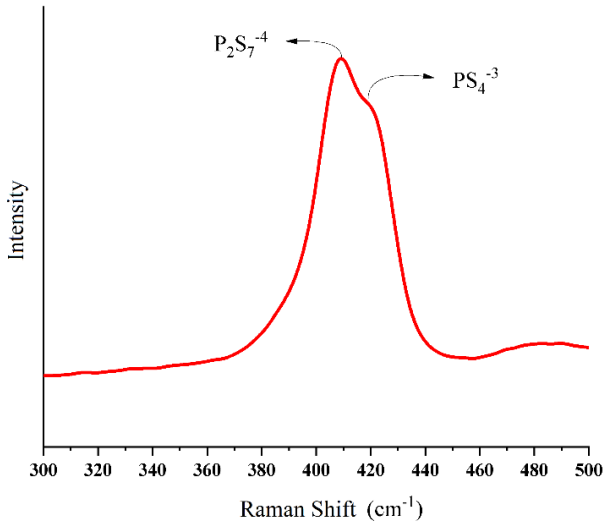

Figure 4. Raman analysis of solid electrolyte.

Glass-ceramics in $P_2S_6^{-4}$ form in the low ionic conductivity phase appear to be 385 cm^{-1}. These peaks are formed as a result of exothermic reactions. The atomic local environment was determined by Raman analysis. The Raman peaks at 405 cm^{-1} and 420 cm^{-1} confirm the formation of Li_7P3S_{11} [9].

Electrochemical impedance spectroscopy (EIS) study was done to measure the ionic conductivity of the obtained solid electrolytes. The molds act as an electrochemical cell at the same time. To avoid air exposure of the materials inside the cell, it is strongly sealed and protected from oxygen or humidity. Impedance measurements were carried out in a symmetrical cell with a solid electrolyte positioned between the two indium (In) electrodes to assess the intrinsic impedance properties of the solid-state electrolyte, unencumbered by the complexities introduced by varying electrode materials or interfaces.

When the impedance curve in Figure 5 is carefully examined, a semicircle and a linear line are clearly seen. Starting point of the semicircle in the X-axis represents the impedance of the solid electrolyte (R_{bulk}). The diameter of the semicircular represents the grain boundary (R_{gb}) and interface resistance (R_{if}) arises between the electrode and electrolyte. The obtainer linear line in the low-frequency region represents the Warburg element (W_o). The ionic conductivity is calculated by finding the total resistance (Eq. 2). $Li_7P_3S_{11}$ powders always have some inclusions that can disrupt the interface and lower the impedance. This resistance is well observed at the intersection at the highest point [9].

$$Total\ Resistance\ R_{total} = R_{bulk} + R_{gb} + R_{if} \quad (2)$$

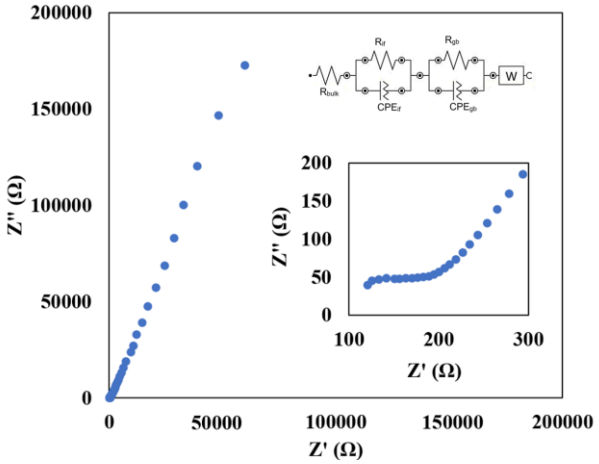

Figure 5. EIS analysis of $Li_7P_3S_{11}$ contained symmetrical cell.

Values of R_{bulk}, R_{gb}, R_{if} calculated using Nova software, were found to be 121.04 Ω, 36.47 Ω, and 27.94 Ω, recpectively. Consequently, the R_{total} was determined to be 185.45 Ω.

The formula for calculating ionic conductivity (σ), as indicated in Eq. 3, is as follows:

$$\sigma = d / (S \times R_{total}) \quad (3)$$

Where: d represents the thickness of the solid electrolyte (in this study, 0.2 cm), and S denotes the contact area (1 cm^2 in this study). Based on these calculations, the total conductivity of the $Li_7P_3S_{11}$ pellet was determined to be 1.1 mS cm^{-1} at room temperature.

The electrochemical stability of $Li_7P_3S_{11}$ was determined by Cyclic Voltammetry (CV) at a scanning rate of 0.1 mV s^{-1}. Electrochemical measurements were carried out in the voltage range of -0.01 V to 4.5 V (Li/Li^+). Cyclic voltammetry curves of Li / $Li_7P_3S_{11}$/ steel asymmetrical cell are shown in Figure 6. It can be easily observed large oxidation and reduction (redox) reactions peaks. The reduction peak, which corresponds to the metallic lithium deposition process ($Li^+ + e^- \rightarrow Li$), is prominently observed at approximately 0 V. Conversely, the oxidation peak linked to lithium dissolution ($Li \rightarrow Li^+ + e^-$) is evident in the voltage range between 0 V and 1 V, and this peak is attributed to the presence of S^{2-} ions [15]. The positions of these peaks closely align with those observed in $Li_7P_3S_{11}$ [9, 24]. The CV analysis also shows that the obtained structure has a wide electrochemical window up to at least 5 V.

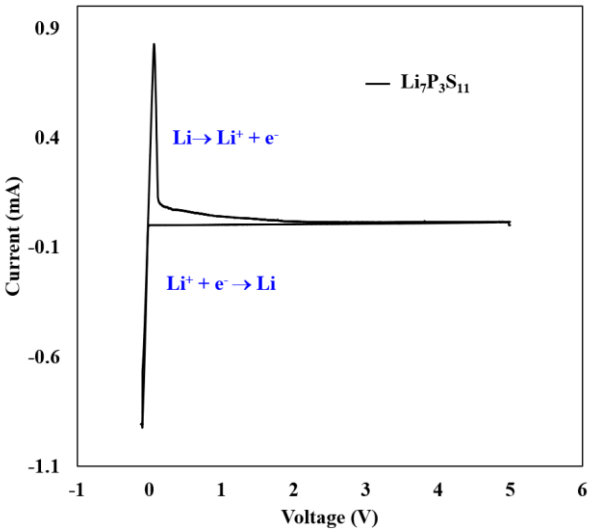

Figure 6. CV analysis of asymmetrical solid-state cell.

When compared to previously documented synthesis methods of $Li_7P_3S_{11}$ solid electrolyte, our approach utilizing ball milling, as illustrated in Table 1, exhibits sufficient ionic conductivity and electrochemical window.

Table 1. Comparison for the electrochemical performance of prepared $Li_7P_3S_{11}$ by ball milling method with other synthesized methods.

Preparation Method	Electrochemical Window (V)	Ionic Conductivity (mS cm^{-1})	Ref
Ball milling	**5**	**1.1**	**This Work**
dissolution-evaporation	5	0.97	[25]
liquid phase process-ultrasonic irradiation	5	1	[26]
optimal laser	-	0.7	[27]

4. CONCLUSIONS

The $Li_7P_3S_{11}$ solid electrolyte intended for use in all-solid-state lithium-sulfur batteries have been effectively synthesized through the mechanical alloying method. Structural analyses were conducted on the acquired powders, revealing that their distinctive properties were consistent with those reported in the literature. Furthermore, the use of thermal analysis methods allowed for accurate determination of crystallization temperatures. Subsequently, the structurally characterized powders were subjected to ionic conductivity testing through impedance measurements within an electrochemical cell. The obtained results have been found to fall within the acceptable thresholds for all-solid-state batteries. Finally, the cell subjected to cyclic voltammetry (CV) testing exhibited reversible oxidation and reduction reactions, maintaining stability across a broad potential range. These findings are anticipated to make a valuable contribution to advancing the commercialization of all-solid-state lithium-sulfur batteries.

Acknowledgements

This work is supported by the Scientific and Technological Research Council of Turkey (TUBITAK) under the contract number 120N492. The authors thank the TUBITAK workers for their financial support.

This work also receives funding from the European Union´s Horizon 2020 research and innovation program (under the grant agreements no. 100825) under the scope of Joint Programming Platform Smart Energy Systems (MICall19).

The authors also thank to Scientific and Technological Research Council of Turkey (TUBITAK) for 2210-C (1649B022107389) funding program.

We also acknowledge support from Research Fund of the Sakarya University under projects no: 2022-7-24-133.

REFERENCES

[1] Gohari, S., et al., Parametric optimization of sulfur@ graphene composites for aqueous and solid-state rechargeable lithium-sulfur batteries. Diamond and Related Materials, 2023: p. 110267.
[2] Olanrele, S.O., et al., Tuning of interactions between cathode and lithium polysulfide in Li-S battery by rational halogenation. Journal of Energy Chemistry, 2020. 49: p. 147-152.
[3] Li, N., et al., From interlayer to lightweight capping layer: Rational design of mesoporous TiO2 threaded with CNTs for advanced Li–S batteries. Carbon, 2019. 143: p. 523-530.
[4] Deng, S., et al., Carbon nanotube-supported polyimide nanoarrays as sulfur host with physical/chemical polysulfide-traps for Li–S batteries. Composites Communications, 2022. 29: p. 101019.
[5] Al Salem, H.I., Electrocatalysis In Li-S Batteries. 2016.
[6] Zhou, J., P. Chen, W. Wang, and X. Zhang, Li7P3S11 electrolyte for all-solid-state lithium-ion batteries: structure, synthesis, and applications. Chemical Engineering Journal, 2022. 446: p. 137041.
[7] Dietrich, C., et al., Lithium ion conductivity in Li 2 S–P 2 S 5 glasses–building units and local structure evolution during the crystallization of superionic conductors Li 3 PS 4, Li 7 P 3 S 11 and Li 4 P 2 S 7. Journal of Materials Chemistry A, 2017. 5(34): p. 18111-18119.
[8] Zhou, J., et al., Wet-chemical synthesis of Li7P3S11 with tailored particle size for solid state electrolytes. Chemical Engineering Journal, 2022. 429: p. 132334.
[9] Xu, R., et al., Preparation of Li7P3S11 glass-ceramic electrolyte by dissolution-evaporation method for all-solid-state lithium ion batteries. Electrochimica Acta, 2016. 219: p. 235-240.
[10] Aoki, Y., et al., Chemical and structural changes of 70Li2S-30P2S5 solid electrolyte during heat treatment. Solid State Ionics, 2017. 310: p. 50-55.
[11] Tsukasaki, H., et al., Direct observation of a non-crystalline state of Li2S–P2S5 solid electrolytes. Scientific reports, 2017. 7(1): p. 4142.
[12] Tsukasaki, H., S. Mori, S. Shiotani, and H. Yamamura, Ionic conductivity and crystallization process in the Li2S–P2S5 glass electrolyte. Solid State Ionics, 2018. 317: p. 122-126.
[13] Kudu, Ö.U., et al., A review of structural properties and synthesis methods of solid electrolyte materials in the Li2S− P2S5 binary system. Journal of Power Sources, 2018. 407: p. 31-43.
[14] Judez, X., et al., Quasi-solid-state electrolytes for lithium sulfur batteries: Advances and perspectives. Journal of Power Sources, 2019. 438: p. 226985.
[15] Rangasamy, E., et al., An iodide-based Li7P2S8I superionic conductor. Journal of the American Chemical Society, 2015. 137(4): p. 1384-1387.
[16] Zhang, Q., et al., Fe 3 S 4@ Li 7 P 3 S 11 nanocomposites as cathode materials for all-solid-state lithium batteries with improved energy density and low cost. Journal of Materials Chemistry A, 2017. 5(45): p. 23919-23925.
[17] Sobolciak, P., M. Karkri, M.A. Al-Maadeed, and I. Krupa, Thermal characterization of phase change materials based on linear low-density polyethylene, paraffin wax and expanded graphite. Renewable Energy, 2016. 88: p. 372-382.
[18] Kissinger, H.E., Differential thermal analysis. J. Res. Natl. Bur. Stand, 1956. 57(4): p. 217.
[19] Borchardt, H.J. and F. Daniels, The application of differential thermal analysis to the study of reaction kinetics1. Journal of the American Chemical Society, 1957. 79(1): p. 41-46.
[20] Smykatz-Kloss, W., Differential thermal analysis: application and results in mineralogy. Vol. 11. 2012: Springer Science & Business Media.
[21] Yersak, T.A., et al., Consolidation of composite cathodes with NCM and sulfide solid-state electrolytes by hot pressing for all-solid-state Li

metal batteries. Journal of Solid State Electrochemistry, 2022. 26(3): p. 709-718.
[22] Long, D.A., The raman effect. 2002: John Wiley & Sons Ltd.
[23] Huang, B., et al., Li3PO4-doped Li7P3S11 glass-ceramic electrolytes with enhanced lithium ion conductivities and application in all-solid-state batteries. Journal of Power Sources, 2015. 284: p. 206-211.
[24] Jung, S.-Y., R. Rajagopal, and K.-S. Ryu, Synthesis and electrochemical performance of (100− x) Li7P3S11-xLi2OHBr composite solid electrolyte for all-solid-state lithium batteries. Journal of Energy Chemistry, 2020. 47: p. 307-316.
[25] Xu, R.C., et al., Preparation of Li7P3S11 glass-ceramic electrolyte by dissolution-evaporation method for all-solid-state lithium ion batteries. Electrochimica Acta, 2016. 219: p. 235-240.
[26] Calpa, M., N.C. Rosero-Navarro, A. Miura, and K. Tadanaga, Instantaneous preparation of high lithium-ion conducting sulfide solid electrolyte Li7P3S11 by a liquid phase process. RSC Advances, 2017. 7(73): p. 46499-46504.
[27] Eatmon, Y., et al., Air Stabilization of Li7P3S11 Solid-State Electrolytes through Laser-Based Processing. Nanomaterials, 2023. 13(15): p. 2210.